Supplementary Information

Electron transfer kinetics on natural crystals of MoS_2 and graphite

Matěj Velický,[*a] *Mark A. Bissett,*[a] *Peter S. Toth,*[a] *Hollie V. Patten,*[a] *Stephen D. Worrall,*[a] *Andrew N. J. Rodgers,*[a] *Ernie W. Hill,*[b] *Ian A. Kinloch,*[c] *Konstantin S. Novoselov,*[d] *Thanasis Georgiou,*[e] *Liam Britnell*[e] *and Robert A. W. Dryfe*[*a]

[a]School of Chemistry, [b]School of Computer Science, [c]School of Materials, [d]School of Physics and Astronomy, University of Manchester, Oxford Road, Manchester, M13 9PL, UK.
[e]BGT Materials Ltd., Photon Science Institute, Oxford Road, Manchester, M13 9PL, United Kingdom.

Email: matej.velicky@manchester.ac.uk; robert.dryfe@manchester.ac.uk

Table of contents

The additional content in this Supplementary Information includes: atomic force microscopy (AFM) measurement, electron transfer kinetics determination, X-ray photoelectron spectroscopy (XPS) and energy-dispersive X-ray spectroscopy (EDX) analyses of the aged and freshly cleaved MoS_2 surfaces.

S1. AFM measurement

AFM was employed to determine the individual and average thickness of the molybdenite and graphite flakes as described in the main text. The thickness of the samples varied between *ca*. 160 – 630 nm for MoS_2 and 50 – 400 nm for graphite, and the mean thickness of all the measured flakes was determined as *ca*. 380 nm for MoS_2 and 150 nm for graphite. An example of an AFM scan on a bulk MoS_2 crystal and its thickness determination is shown in Fig. S1.

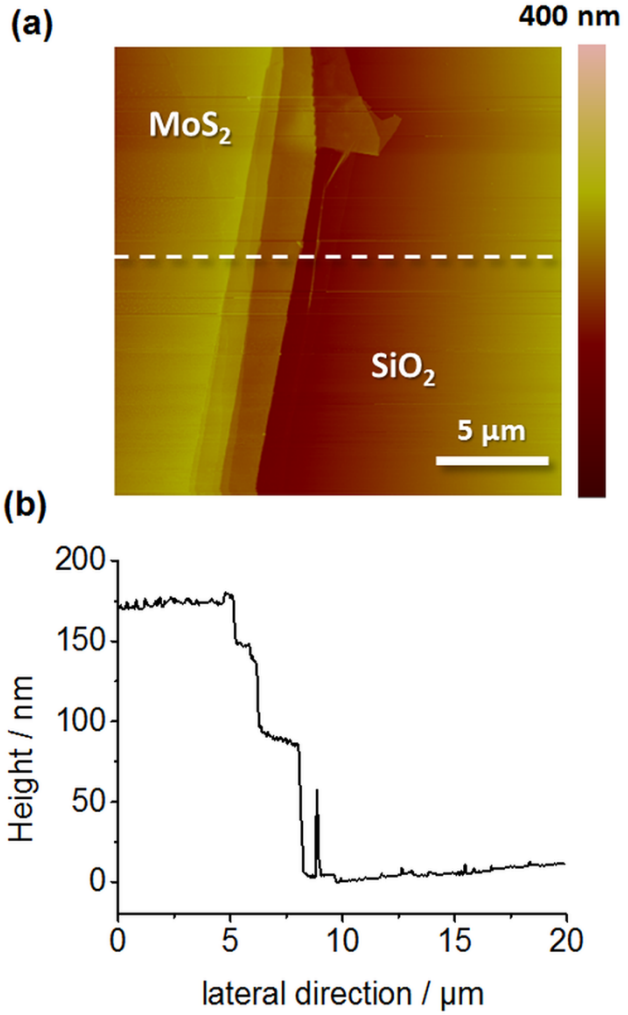

Fig. S1 (a) Representative AFM scan of a MoS_2 flake edge deposited on oxidized silicon substrate. The dashed line indicates the cross-section of the (b) corresponding height profile.

S2. Electron transfer kinetics determination from voltammetry

The current-potential curve, cyclic voltammogram, yields two peaks corresponding to the reduction and oxidation of the redox mediator and the peak-to-peak separation, ΔE_p, was used to determine the standard HET rate constant, k^0. The method of Nicholson,[1] applicable to ΔE_p < 220 mV, is based on the following equation:

$$\psi = k^0 \sqrt{\frac{RT}{\pi nFD}} \nu^{-0.5} \tag{S1}$$

where ψ is the dimensionless kinetic parameter calculated from ΔE_p,[1, 2] R is the universal gas constant, T is the thermodynamic temperature, n is the number of electrons involved in the reaction, F is the Faraday constant, D is the diffusion coefficient (assumed similar for both reduced and oxidized forms of the mediator) and ν is the scan rate. Eq. (S1) was used to determine k^0 from the slope of $\psi - \nu^{-0.5}$ dependence (for ΔE_p < 220 mV). The kinetic parameter ψ was calculated from ΔE_p using the empirically determined working function:[2]

$$\psi = \frac{(-0.6288 + 0.0021\, n\, \Delta E_p)}{(1 - 0.017\, n\, \Delta E_p)} \tag{S2}$$

An explicit expression for k^0 given by Klinger and Kochi,[3] was used to find k^0 for ΔE_p > 220 mV:

$$k^0 = 2.18 \left(\frac{\alpha\, n\, F\, D \nu}{RT} \right)^{1/2} e^{-\frac{\alpha^2 F}{RT} n \Delta E_p} \tag{S3}$$

where α is the transfer coefficient, assumed to be 0.5 for a symmetrical reaction. Both Eq. (S1) and (S3) are only valid for one-electron transfer processes (n = 1). A range of scan rates from 1 V s $^{-1}$ down to 100 mV s $^{-1}$ (1, 0.8, 0.6, 0.4, 0.3, 0.25, 0.2, 0.15 and 0.1 V s $^{-1}$) were recorded for each micro-droplet. The average k^0 was determined as an arithmetic mean of values obtained either from Eq. S1 and S2 (for ΔE_p < 220 mV) or Eq. S3 (for ΔE_p > 220 mV).

S3. XPS and EDX spectroscopy of the aged and freshly cleaved MoS_2 surface

XPS analysis

The data in Table S1 show how the elemental composition varies at 5 different surface sites of atmosphere-aged and freshly cleaved MoS_2 as determined from XPS analysis (full spectra are shown in Fig. 5 of the main text). The elemental analysis reveals that, apart from molybdenum and sulphur, there is a significant amount of carbon and oxygen on the surface (*ca*. 28 – 34 at. % combined), and a small amount of other impurities such as Si, Fe and Bi (*ca*. 1 – 4 at. % combined). Overall, the Mo and S atoms constitute *ca*. 71 at. % of the cleaved surface, which decreases to 62 at. % for the aged surface. The S/Mo ratio (1.7 – 2.1) is close to the expected value of 2 in MoS_2. The level of impurity is quite high when compared to graphite (92.8 – 93.2 at. % carbon content).[4] This can be explained by the ubiquitous adventitious carbon adsorption on most air-exposed surfaces,[5] which is naturally much harder to detect on graphite. Furthermore, the similar concentration of adventitious carbon on aged and cleaved surface suggests that the contamination of the surface with hydrocarbon and/or graphitic impurities occurs very rapidly within the time-window between exfoliation of a fresh surface and XPS measurement, *i.e*. within minutes or even seconds.

Table S1 Variation in the elemental composition of the aged and cleaved MoS_2 surface, determined from XPS analysis.

element	surface site variation / at. %		average / at. %	
	aged	cleaved	aged	cleaved
C	16.84 – 22.05	16.23 – 29.12	19.76	20.91
O	10.72 – 20.70	4.44 – 10.19	14.46	7.23
Si	1.63 – 5.65	0.00 – 2.37	3.18	1.16
S	35.87 – 47.46	36.51 – 48.36	42.13	44.71
Fe	0.00 – 0.31	< 0.01	0.10	< 0.01
Mo	18.63 – 22.98	21.37 – 28.38	20.12	25.99
Bi	0.00 – 0.44	< 0.01	0.25	< 0.01

In comparison to MoS_2, both aged and cleaved graphite on average contain much less surface oxygen (4-5%) but similar amounts of non-graphitic sp^3 adventitious carbon contamination (*ca*. 20-25%) as MoS_2, as determined by XPS.[4] As well as the wide range XPS spectra seen in Fig. 5 (main text), high resolution spectra of the sulphur 2p and molybdenum 3d shells were taken for both freshly cleaved and aged samples of MoS_2 as shown in Fig. S2.

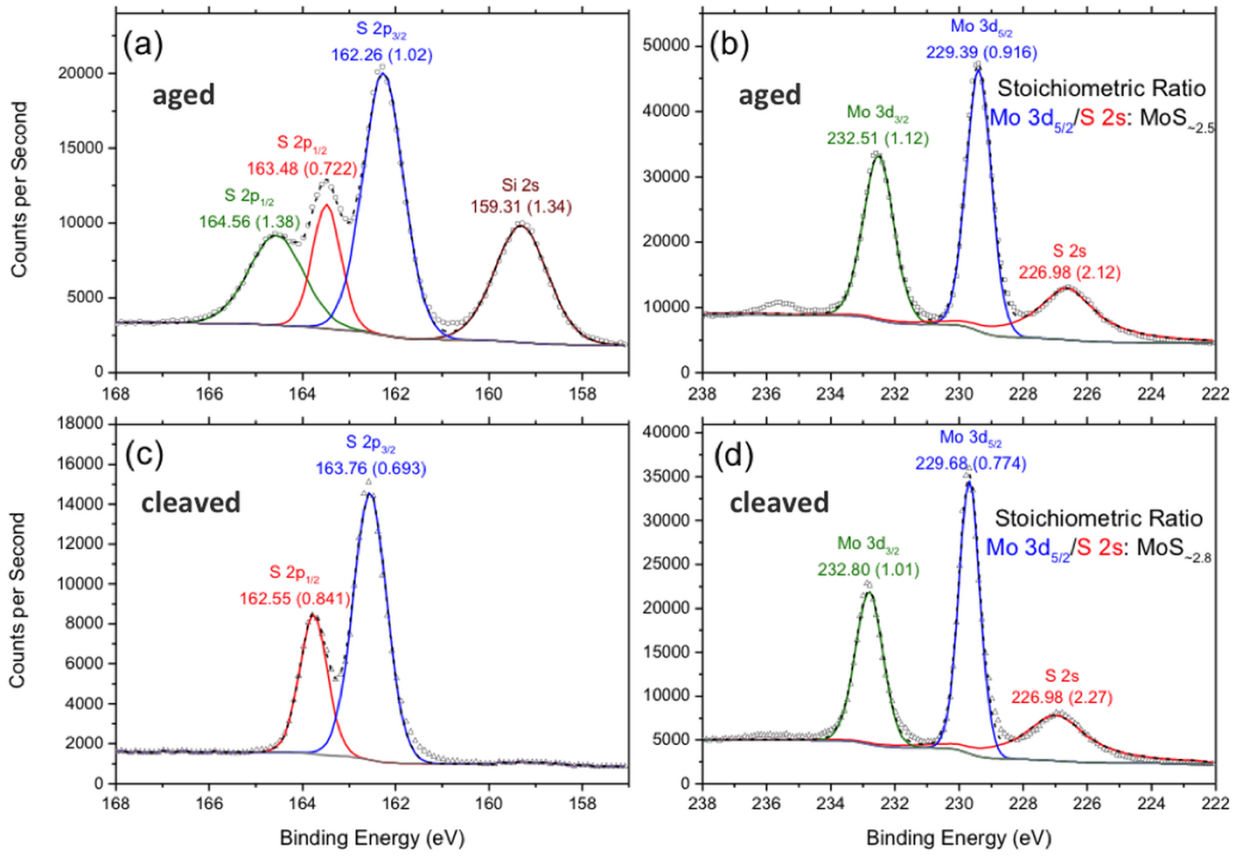

Fig. S2 High-resolution XPS spectra showing (a) S 2p and (b) Mo 3d shells of the aged, and (c) S 2p and (d) Mo 3d shells of the freshly cleaved MoS_2 substrates. Each of the peaks is labelled with the corresponding shell, as well as the binding energy, and full width at half maximum in parentheses.

Fig. S2a and Fig. S2b are of the aged MoS_2 and differ significantly when compared to the freshly cleaved sample (Fig. S2c-d). The S 2p doublet (S $2p_{3/2}$ and S $2p_{1/2}$) in Fig. S2a has split into a third peak which has previously

been attributed to partial oxidation of the MoS_2 lattice,[6] agreeing with the elemental composition (Table S1) that shows increased oxygen content of the aged sample. The amount of generic surface contamination is also much larger as noted by the silicon 2s peak being resolved. Fig. S2b shows the Mo 3d peaks (Mo $3d_{5/2}$ and Mo $3d_{3/2}$) along with the S 2s peak. The binding energies of the Mo doublet are similar to the expected values and the freshly cleaved spectra, however a small peak is partially resolved at *ca*. 235.8 eV which can be attributed to molybdenum having an octahedral co-ordination (Mo^{6+}) occurring upon partial oxidation of Mo^{4+}.[6] The appearance of this peak is in accordance with the higher concentration of oxygen in the aged sample. Note, however, that the Mo 3d doublet peaks do not show the typical metal-oxide shoulder at high binding energy side of the peaks, which would be expected as a result of surface oxidation. It has been suggested, that the oxygen contamination of the surface can occur via oxygen atom adsorption on the ubiquitous sulphur vacancy defects on the MoS_2 surface.[7] Small amount of oxidation detected from high-resolution XPS peaks and also much lower overall oxygen concentration determined from EDX (see below) suggests that the oxidation of MoS_2 only occurs in the uppermost layers of the crystals.

Fig. S2c (freshly cleaved sample) shows the spectra with the sulphur 2p doublet clearly resolved and at binding energies closely matching the expected values for MoS_2.[6] From the position, relative intensities, and shape of the S 2p peaks we can determine that MoS_2 was predominantly the semiconducting 2H phase.[8] Finally, Fig. S2d (freshly cleaved sample) shows both the molybdenum 3d region, as well as the sulphur 2s peak, closely matching the expected values.

EDX analysis

Comparison of the EDX spectra obtained on both atmosphere-aged and freshly cleaved MoS_2 samples and the electron micrographs of the analysed areas are shown in Fig. S3 and S4, respectively. The elemental analysis confirms the same main constituents (Mo, S, C and O) as XPS analysis and also other impurity elements (F, Al, Si, K, Fe and Bi, less than 1.7 – 2.4 at. % combined).

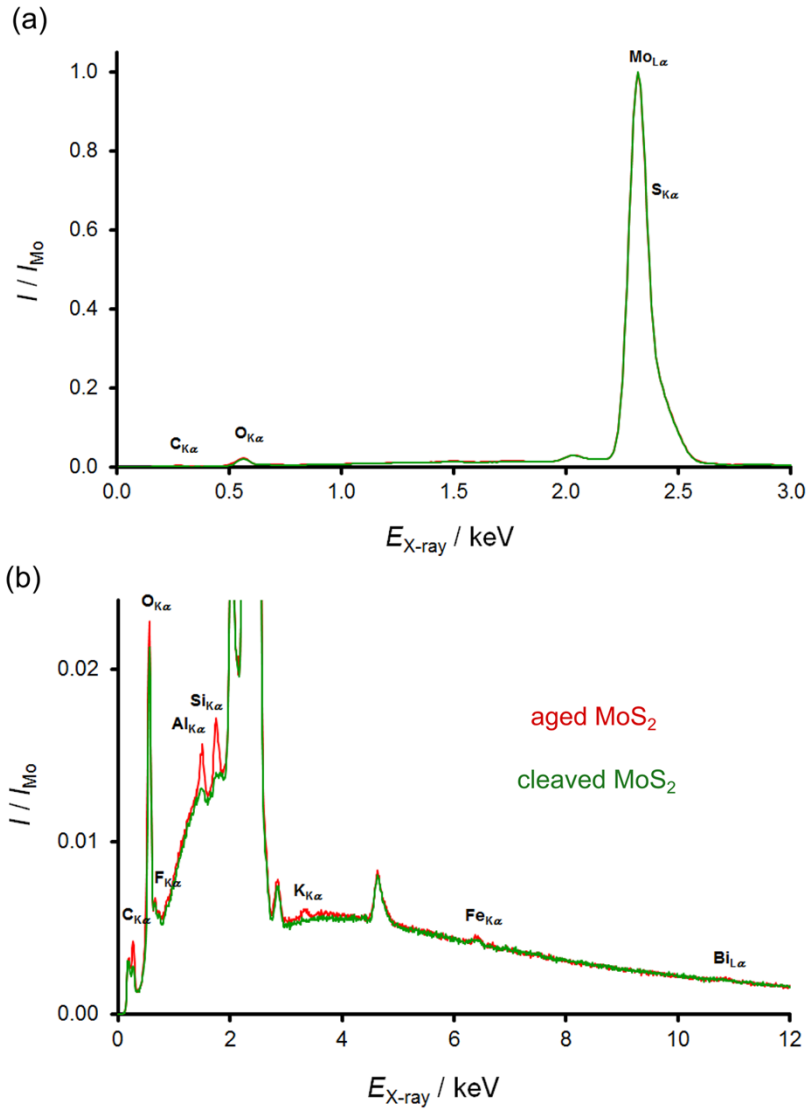

Fig. S3 Comparison of the EDX spectra recorded on aged (red) and cleaved (green) MoS_2 surface. The spectra show (a) the four main constituents, Mo, S, O and C and (b) the impurity elements in detail. Both intensity scales are normalized to intensity of the $Mo_{L\alpha}$ peak.

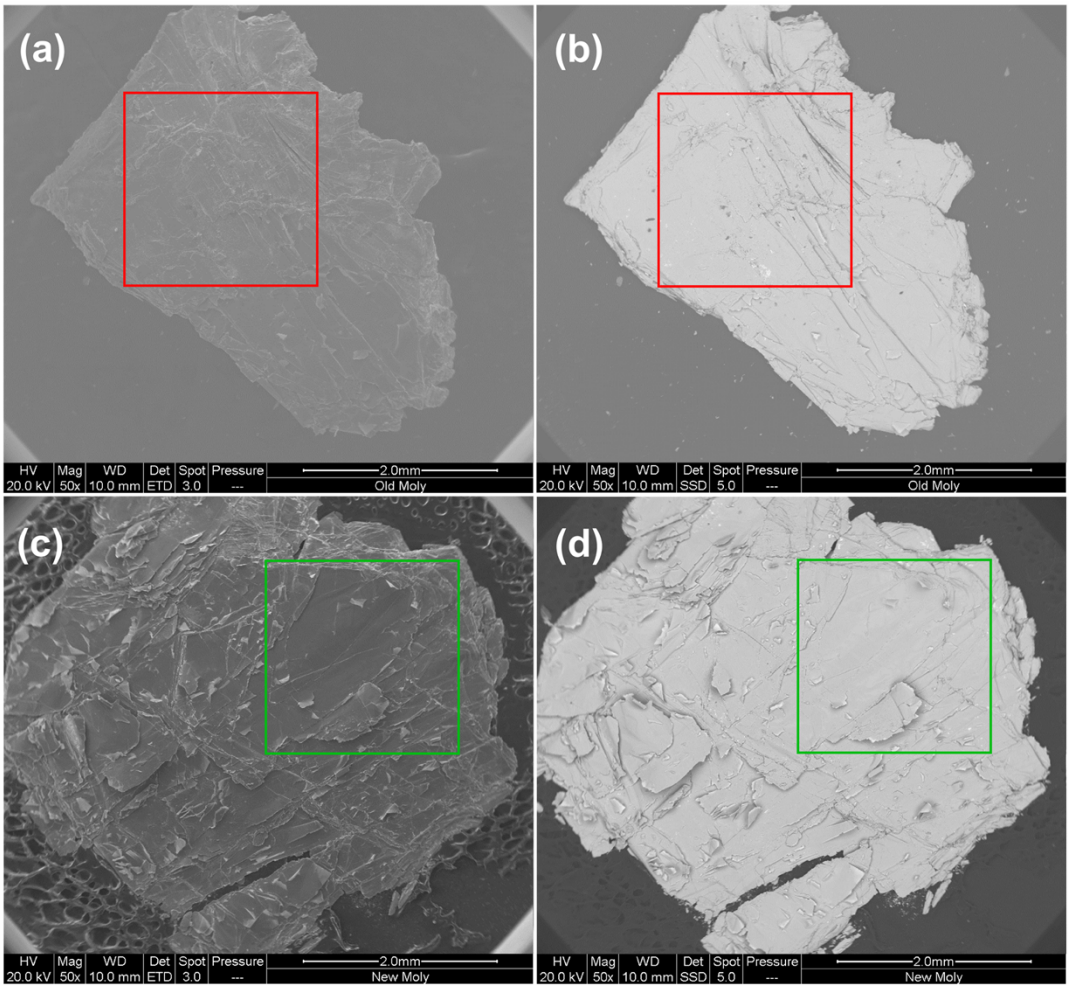

Fig. S4 Electron scanning micrographs indicating the areas on MoS_2 crystals used for EDX quantification. (a) and (b) are the secondary and backscattered electron micrographs of the aged surface, respectively, (c) and (d) are the secondary and backscattered electron micrographs of the freshly cleaved surface, respectively.

In comparison to XPS measurement, the combined amount of the two main contaminants, carbon and oxygen, is lower: *ca*. 15.8 – 22.4 at. %, and the overall concentration of Mo and S atoms reaches 75 and 82 at. % for the aged and cleaved surface, respectively. XPS is a surface-sensitive method whereas EDX provides more information about the bulk MoS_2 material. This observation therefore suggests that the oxidation and hydrocarbon contamination is limited to a thin layer at the surface of the material. Note that the S/Mo ratios vary between 2.4 – 2.8, which is most likely a consequence of the overlapping peaks of molybdenum and sulphur in the EDX spectrum, which adversely affects the quantification.

Table S2 Elemental composition of MoS_2 crystal determined using EDX analysis of a 4 mm^2 area on aged and cleaved surface.

element	aged / at %	cleaved / at %
C	10.23	6.91
O	12.21	8.92
F	1.26	1.25
Al	0.34	0.14
Si	0.35	0.26
S	53.26	60.75
K	0.06	0.00
Fe	0.10	0.08
Mo	21.96	21.68
Bi	0.24	0.00

References

1 R. S. Nicholson, *Anal. Chem.*, 1965, **37**, 1351-1355.

2 I. Lavagnini, R. Antiochia and F. Magno, *Electroanalysis*, 2004, **16**, 505-506.

3 R. J. Klingler and J. K. Kochi, *J. Phys. Chem.*, 1981, **85**, 1731-1741.

4 M. Velický, D. F. Bradley, A. J. Cooper, E. W. Hill, I. A. Kinloch, A. Mishchenko, K. S. Novoselov, H. V. Patten, P. S. Toth, A. T. Valota, S. D. Worrall and R. A. W. Dryfe, *ACS Nano*, 2014, **8**, 10089-10100.

5 T. L. Barr and S. Seal, *J. Vac. Sci. Technol., A*, 1995, **13**, 1239-1246.

6 L. Benoist, D. Gonbeau, G. Pfister-Guillouzo, E. Schmidt, G. Meunier and A. Levasseur, *Thin Solid Films*, 1995, **258**, 110-114.

7 H. Nan, Z. Wang, W. Wang, Z. Liang, Y. Lu, Q. Chen, D. He, P. Tan, F. Miao, X. Wang, J. Wang and Z. Ni, *ACS Nano*, 2014, **8**, 5738-5745.

8 G. Eda, H. Yamaguchi, D. Voiry, T. Fujita, M. Chen and M. Chhowalla, *Nano Lett.*, 2011, **11**, 5111-5116.